TRIUMF Experiment E614
Technical Note 54

TWIST Detector and Systematic Error Estimations

V.I. Selivanov

29 August 2001

Abstract

The following note is a sixth analysis of the systematic errors of the E614. Previous ones have been done in 1991 (Original E614 Proposal), 1992 (Report, unpubished), 1994 (Review, unpublished), 1997 (E614 Project Proposal), 1998 (E614 Project Proposal). The given note is based on many Technical Notes that were done by the E614 team after the last Project Proposal. The Michel parameter error estimations practically are not changed: $\sigma(\mathrm{P}_\mu\xi) = [\pm 10(\mathrm{stat}) \pm 8.5(\mathrm{syst})]\cdot 10^{-5}, \sigma(\rho) = [\pm 5(\mathrm{stat}) \pm 7.0(\mathrm{syst})]\cdot 10^{-5}, \sigma(\delta) = [\pm 8(\mathrm{stat}) \pm 6.4(\mathrm{syst})]\cdot 10^{-5}$.

1. Detector Description

Schematic layout of the E614 detector assembly to be inserted into the magnet is presented in Fig.1 together with sample positron helices in a B = 2.35T at energies 30 and 53MeV and polar angles $\theta = 5^\circ, 10^\circ, 60^\circ$. Surface muons from M13 channel going along Z$-$axis and stop in a target at center of the assembly. Gas degrader placed upstream of the scintillator detector. Muon counter (TEC) placed at Z=$-$140cm outside of the iron shield close to the input window.

• The stopping target is a thin $\approx 20\mathrm{mg/cm}^2$ foil from a material with low Z of nucleus to reduce radiation losses of outgoing positrons. Foils from Be, graphite, Al, and aluminized mylar will be used. About 75% of surface muons stop inside the target [1]. Cross-section of the stopped muon beam has $\sigma_\mathrm{x} \approx \sigma_\mathrm{y} \approx 7.5$mm at B = 2T. The target also serves as a cathode plane for proportional chambers PC($-$1) and PC(+1).

• Identical (X+Y) PC pairs (central PCs) on both sides of the stopping target are indicators and coordinate detectors of muon stops inside the target. A "fast" drift gas CF_4/ISO(80/20) is used. Scatterplot of energy losses in PC($-$2) and PC($-$1) has different distributions for muons stopped in PC($-$1) gas and the target (see Fig.2) [2]. Amplitude analysis of the energy loss in PC($-$2) and PC($-$1) provides for rejection at level $< 0.6\%$ muons stopped in PC($-$1) gas and excludes influence of a muon depolarization by PC($-$1) gas on P_μ value. Center of gravity of muon stopping distribution inside the target along Z axis has defined with accuracy $\pm 1\mu$m by muon ratio $N_{PC(-2)}/N_{PC(+2)}$ or $N_{PC(-1)}/N_{PC(+1)}$ [2]. All wires of the PCs instrumented therefore by TDC and ADC outputs

• 20mm helium gap between the central PCs and the PDC pair closest to the target is introduced for better separation of an ingoing muon from outgoing upstream small polar angle positrons.

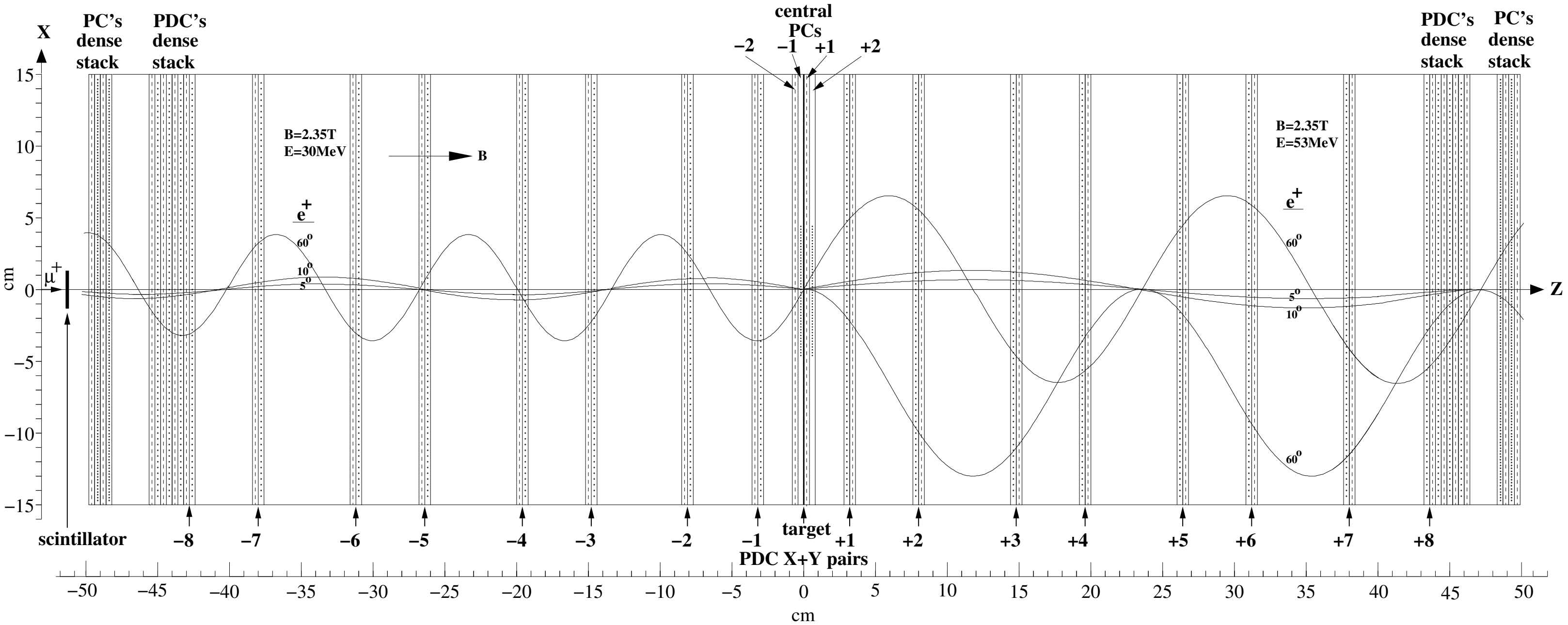

Figure 1: Schematic layout of the detector assembly.

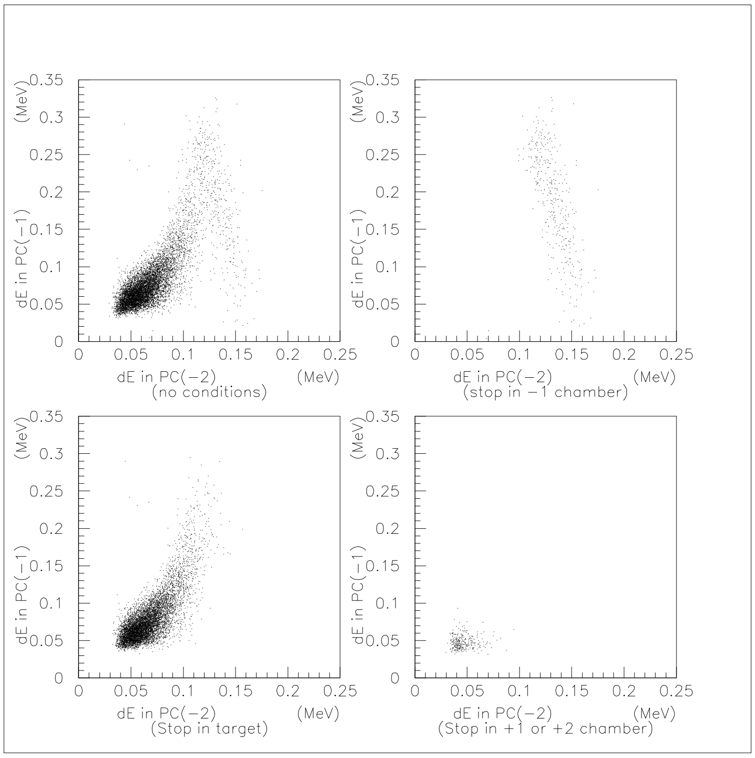

Figure 2: Energy loss in (PC − 2) and (PC − 1) chambers for various conditions. Top left: no conditions; top right: stop in (PC−1); bottom left: stop in target; bottom right: stop in in PC(+1) or PC(+2)

• Eight pairs ($\pm1, ..., \pm8$) of (X+Y) PDC planes measure positron helices. They are interleaved by 40 or 60mm helium gaps introduced to improve detector resolution at small angles. "Slow" and "cold" drift gas, DME (C_2H_6O) is used in all PDCs to decrease an influence of Lorentz drift angle at the magnetic field B = 2T on a shortest reconstructed distance between positron helix and sense wire.

• Dense PDC stacks serve as an additional tool for identification of a positron helix with period around 4mm. This helix crosses all PDC planes at identical (X, Y) coordinates, and imitates therefore a straight line with polar angle $\theta = 0$.

• Dense PC stacks serve as a zero time master with 2.5ns (RMS) resolution [3] for the outgoing positron helix registration. A "fast" drift gasCF_4/ISO(80/20) is used.

• Upstream and downstream parts of the detector are mirror symmetrical relative to the target plane excluding the central PCs. The [PC(−1X)− target−PC(+1Y)] geometry is selected to decrease a crosstalk between the planes, especially from a muon stopped in the target and producing a big signal in PC(−1X).

• Plastic scintillator serves for muon identification. It is 0.25mm thick by 25mm diameter Bicron. A Bicron fiber wavelength shifter 1mm in diameter was wrapped around the scintillator diameter. The ends of the fiber extended approximately 1m away from the scintillator and coupled to two PMTs. The time resolution of this assembly is less than 2ns [4].

• An 18cm long variable gas degrader allows control over the muon stopping distribution by varying the CO_2/He mixture [5].

• Muon counter [5, 6] is a time expansion chamber (TEC) working at DME gas pressure P=20−40torr in order to restrict a multiple scattering of surface muons. The TEC allows measurement of each muon trajectory with space error $\approx 50\mu$m and angle error $\approx$ 5mrad.

• Detailed detector specification is presented in Table 1.

Table 1: Basic parametrs of the E614 detector

	PC	PDC
Diameter of (W/Re)Au sense wires	15μm	
Wire spacing	2mm	4mm
Gap between wire and cathode	2mm	
Cathode plane	Double-side 6μm aluminized mylar	
Drift gas	CF_4/ISO(80/20)	DME(C_2H_6O)
Gas between PDC (PC) modules	He + 5%N_2	
Number of planes	12	44
Number of wires per plane	160	80
Total number of wires	1920	3520
Working diameter of the detector	320mm	
Gas pressure	760 Torr	
Temperature	20°C	

2. Peculiarities of the E614 Detector

• An attempt to measure separately any Michel parameter with accuracy of 10^{-4} requests an independent knowledge of other parameters with the same precision because any part of muon decay spectrum is described by more than one parameter. For example, accuracy of world value ρ restricts the measuring value of δ at level of $\pm 1.1 \cdot 10^{-3}$ [7]. Only Michel parameters combination $P_\mu \xi \delta / \rho$ does not depends on rest Michel parameter η. The combination was measured with precision of $\pm 3 \cdot 10^{-3}$ [8]. We have no idea how one could improve the last result using a similar detector. Thus, because all Michel parameters are known with accuracy of $\pm 10^{-3}$, we have proposed a detector design to measure with accuracy about 10^{-4} the all Michel parameters simultaneously. The proposed detector measures 3D positron spectrum from muon decay at energy limits $x = 0.1 - 1$, polar angle of $0.5 < cos\theta < 0.985$ and any azimuthal angle φ. Here x is reduced positron energy E/E_{max}, where $E_{max} = (m_\mu^2 + m_e^2)/2m_\mu$ = 52.8304MeV is the maximum positron energy and m_μ and m_e are the particle masses. One needs to remark that it will be a *first attempt to measure the differential* $d^2N/dxdcos\theta$ *positron spectrum* after more than 30 years of muon decay study. All most accuracy previous experiments [7, 8, 9] have measured a dN/dx spectrum inside some solid angle. For example, the systematic error of δ was $\pm 1.1 \cdot 10^{-3}$[8] because an uncertainty of the solid angle.

The Michel parameters $\rho, \eta, P_\mu \xi, \delta$ will be defined from the full spectrum $d^2N/dxdcos\theta =$

$N_1(x,\rho,\eta) \pm N_2(x,\delta) P_\mu \xi cos\theta$. The upstream and downstream part of the detector registers $N_{up} = N_1 + N_2 P_\mu \xi cos\theta$ and $N_{down} = N_1 - N_2 P_\mu \xi cos\theta$ correspondingly for a surface muon beam with $P_\mu = -1$. Analysis of $N_+ = N_{up} + N_{down} = 2N_1(x,\rho,\eta)$ gives possibility to measure ρ and η parameters independently from $P_\mu\xi$ and δ. Similarly the $N_- = N_{up} - N_{down} = 2N_2(x,\delta) P_\mu cos\theta$ allows a measurement of $P_\mu\xi$ and δ independently from ρ and η. Analysis of the N_{down} around $x = 0.5$ where $P_\mu\xi \approx 0$ gives possibility to measure parameter δ as it was done in reference [7]. Fitting of the N_{down} in area with $x \to 1$ and $\cos\theta \to 1$ allows a measurement of $P_\mu\xi\delta/\rho$ as it has been done in reference [8]. Analysis of the N_{up} in area with small values of x repeats the experimental design of reference [9]. Furthermore the all Michel parameters can be measured from N_{up} and N_{down} separately. All the possibilities of the differential spectrum $d^2N/dxdcos\theta$ improve of course reliability of the measured Michel parameter values.

• The proposed detector is a linear system in a homogeneous magnetic field. Such system requests only one point for energy calibration. The maximum energy of positron $x = 1$ in muon decay can serve as the calibration point which be contained in the Michel spectrum itself. Needed statistics accuracy of the calibration about ±10keV corresponds to statistics of $2 \cdot 10^6$ of positrons into 4π solid angle according to Monte Carlo estimation for the E614 detector. External sources were used in references [7, 8, 9] for the energy calibration. As result, corresponding systematic error of δ was $2 \cdot 10^{-3}$ in [7] and $5.5 \cdot 10^{-4}$ for $P_\mu\xi\delta/\rho$ in [8].

• A new technique of a helix reconstruction is suggested. We named it *"sliding"*. The positron is tracked by EGS4 through the full E614 detector upstream from the target. The helix is then fitted sequentially using subsets of four (X+Y) PDC pairs (Fig.1) 1234, 2345, 3456, 4567, and 5678. We shall call each such pair subset a *slide*. The fit result will be retained (selected) for a slide with the maximum confidence level value (χ^2 is not used for the selection because the number of wire hits in slides varies from slide to slide). Thus, the total statistics will be distributed between the slides. One can see from Fig.3 [10] that the sliding technique completely removed events with CL ≈ 0, which constitute about 20% of events in the "raw" case. *The sliding technique gives a statistical correct value of* $<\mathrm{CL}>> 0.5$ and that provides therefore most important advantage of the technique. Price of the technique using is sufficient increasing of wire channel number. Energy and angle resolution of the detector is presented in Fig.4 [10].

• The peculiarity of the proposed detector is defined by its planar geometry. A planar target and the assembly of planar chambers (PCs and PDCs) are arranged perpendicular to the magnetic field (Fig.1). In such layout the mean energy loss of particles in the detector is given by $\mathrm{dE(E,\theta)/dz = [dE(E,\theta=0)/dz]/cos\theta}$. This formula simply expresses the fact that the effective degrader thickness (path length) grows as the $1/\mathrm{cos}\theta$. The $1\ /\mathrm{cos}\theta$ dependence is obvious for the planar target, for a gas gap and for the planar cathode plane. It also applies to wires even though loss does not have this simple dependence on θ (for cylindrical wires) since the probability of hitting a wire does have a $1/\mathrm{cos}\theta$ dependence on θ also. This dependence was investigated by Monte Carlo simulation [10]. Simulation positron source with energy $\mathrm{E_0} = 50\mathrm{MeV}$ was uniformly distributed over a 20mm diameter within the $20\mathrm{mg/cm^2}$ stopping Al target. Fig.5 shows the dependence of the mean reconstructed positron energy $<\mathrm{E_{fit}}>$ on entrance of PDC module # +1 after passing by positron of Al

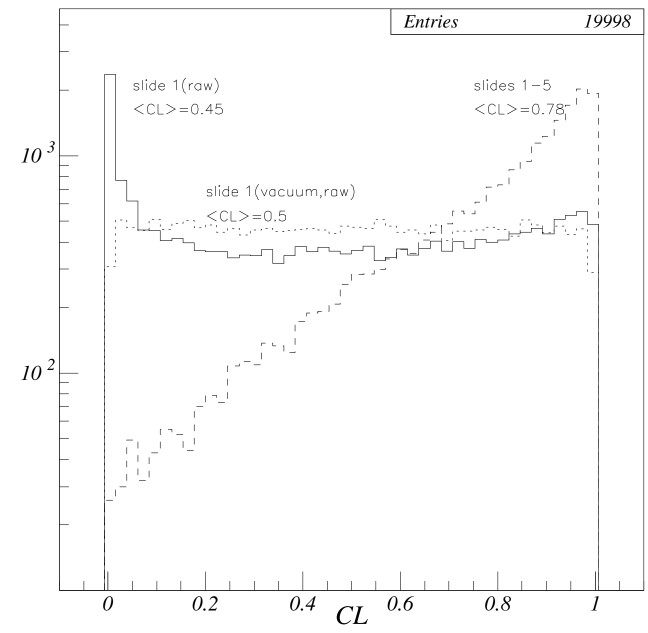

Figure 3: Confidence level (CL) distribution for reconstructed events. Initial positron energy 50MeV, initial polar angle $\cos\theta = 0735$. PDC space resolution is 50μm. "Slide 1(raw)" is the result of the first slide (1234) fitting. "Slides 1−5" present the same events that were fitted with slide selection and resulting distributions of all five slides were summed. The flat distribution with $< \mathrm{CL} >= 0.5$ corresponds to the fit of vacuum helices with 50μm PDC resolution.

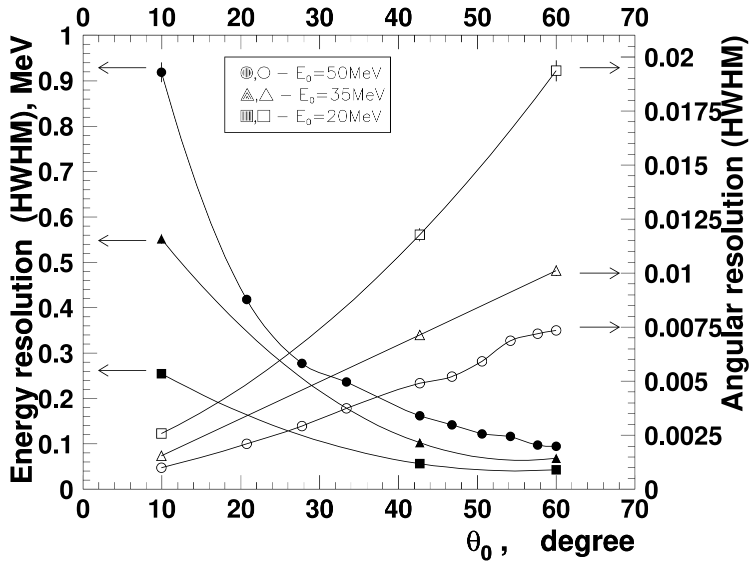

Figure 4: Energy HWHM $= 1/2 \cdot \mathrm{FWHM}(\mathrm{E_{fit}} - \mathrm{E_0})$ and angle HWHM $= 1/2 \cdot \mathrm{FWHM}(\cos\theta_{\mathrm{fit}} - \cos\theta_0)$ resolutions at different initial positron energies.

target, two PC chambers, He gap between the PCs and PDC, first cathode plane of the first PDC. As one can see, it can be parameterized with a linear function $<\mathrm{E_{fit}}>= \mathrm{E_1} - \alpha/\cos\theta$, where $\mathrm{E_1}$ is the initial positron energy at a muon decay point and α is the positron energy loss at $\theta = 0$. The straight line fits to each slide data points are presented on Fig.5. The net result is: $\Delta \equiv E_1 - E_0 =< E_{fit} > -E_0 = (-2.2 \pm 2)$keV for extrapolation to $1/\cos\theta = 0$. *It means we can reconstruct an original energy of a decaying positron at any angle θ, without knowledge of its energy losses before the coordinate detector.* The 1/cosθ dependence is violated by scattering and radiative interactions with the detector matter. Non-conservation of the mean value of cosθ in the E614 detector is less than $6 \cdot 10^{-5}$ for 20mg/cm^2 of Be target at $cos\theta = 0.5$ and $E_0 = 20$MeV, and it is about $2 \cdot 10^{-5}$ at $E_0 = 50$MeV (see Fig.11 in reference [10]). The energy calibration will not be restricted to this $x \to 1$ point but can be assumed to apply over the energy range $0.4 < x < 1$ since the E614 detector is a linear detection system because of the homogeneous magnetic field.

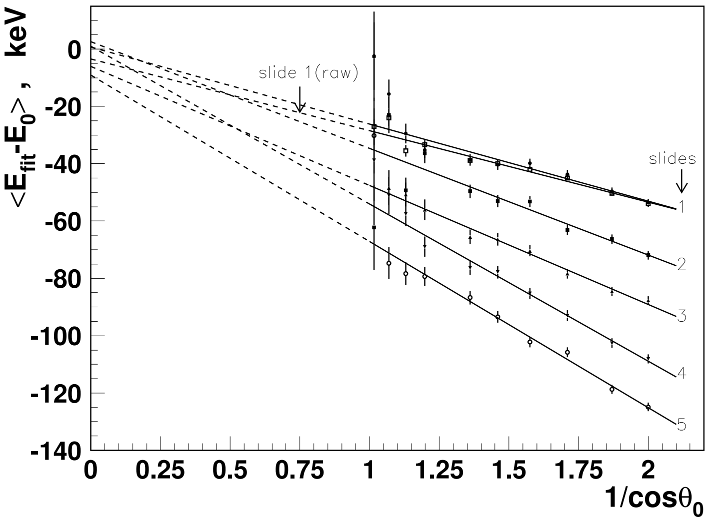

Figure 5: Mean reconstructed positron energy $< E_{fit} >$ as a function of $1/\cos\theta_0$. $E_0 = 50$MeV, $\sigma_{PDC} = 50\mu$m. Straight lines are the fits with function $< \Delta E_{fit} >= E_0 - \alpha/\cos\theta_0$.

• Amplitude analysis of signals from PC(-2) and PC(-1) provides reliably identification of muon stopped in a target with thickness of 20mg/cm^2 only (see Fig.2). An outgoing positron passes in average 12mg/cm^2 of matter before the entrance of first PDC plane. It corresponds to $\approx$30keV of energy loss before the coordinate detector, compare with 240mg/cm^2 ($\approx$0.6MeV correspondingly) in most precise previous experiments [7, 8]. A possible distortion of the original Michel spectrum by the energy loss will be much smaller in the E614 detector than in previous ones [7, 8].

• The longitudinal magnetic field B=2T is sufficient to keep a thermalized muon polarization as that will be estimated below.

• The proposed goal to measure Michel parameters $\rho, P_\mu\xi, \delta$ at level of 10^{-4} accuracy requests to measure the Michel spectrum by the E614 detector with a systematic energy shift $\Delta E < 10$keV and angle shift $\Delta\theta < 5 \cdot 10^{-4}$ according to our previous Monte Carlo estimations. We need to design and manufacture a precise drift chamber assembly for the positron registration. An influence of the detector imperfections on reconstructed Michel parameters is estimated below.

3. Systematic Error Estimations

3.1. M13 beam line

3.1.1.Coulomb scattering of muons inside the production target.
The production of surface muons has been modeled in a routine based on GEANT (see Fig.4 in [11]). Muon depolarization was calculated versus depth of decaying muon from the 1AT1 target surface. The M13 channel with a central momentum of 29.6MeV/c and the momentum acceptance of $\pm 0.5\%$ captures of muons from a maximal depth of 20μm. It corresponds to the average value of $(1 - \mathrm{P}_\mu) = 9 \cdot 10^{-5}$ of the muon beam. The central beam momentum stability is $\Delta \mathrm{p}/\mathrm{p} = 0.03\%$ (see 3.1.4). It corresponds to $(1 - \mathrm{P}_\mu) = 10^{-5}$. We will accept a pessimistic estimation $(1 - \mathrm{P}_\mu) = (9 \pm 2) \cdot 10^{-5}$.

3.1.2. Non-surface muon contamination.
Impurities in the surface muon beam, that is, any particle that is not a surface muon , may be a source of positrons that, if mistakenly identified as originating from the decay of a polarized surface muon would distort the Michel spectrum. The impurities at p_0=29.6MeV/c, given in Table 2 were determined in a test run in 1995.

Table 2: M13 surface μ^+ beam impurities per surface muon (PSM).

Contaminant Particle	Measured rate/surface muon
e^+	4
π^+	$2.9 \cdot 10^{-3}$
μ^+(cloud) from 1AT1 (graphite)	$2.1 \cdot 10^{-2}$
μ^+(cloud) from S0	$3.4 \cdot 10^{-4}$
μ^+(non-surface) in "usable" window	$6.7 \cdot 10^{-5}$

Positrons from M13 easy distinguish from a surface muon because the positrons go through full detector assembly near Z$-$axis. Probability to coincidence of a positron from the channel with an outgoing decaying positron is about 12% inside 10μs window at muon intensity of $3 \cdot 10^3 \mathrm{s}^{-1}$. First of all, one can exclude the overlapping events from the Michel spectrum, as that one does in μSR-technique. Second one, we not see difficulties to reconstruct the both positrons. Influence of the contamination on Michel parameters is negligible therefore.

Most part of π^+ captured by the M13 stops in scintillator and the upstream PCs and PDCs dense stacks before the stopping target because range of π^+ is less on 70mg/cm^2 than surface muon range ($\approx$ 150mg/cm^2). Muons from the decaying pions have the momentum 29.8MeV/c and they are uniformly distributed in 4π solid angle. The muons with a polar angle $\theta > 20^\circ$ can be measured by the upstream PDC pairs and rejected therefore. Rest part of the muons with $\theta < 20^\circ$ can imitate surface muons from M13 channel. Their percentage is about 1%. These muons can stop in the target and do a total admixture to true surface muons about $1\% \cdot 2.9 \cdot 10^{-3} = 2.9 \cdot 10^{-5}$. Let us remark here that the muons will have polarization $(1 - \mathrm{P}_\mu) < 1 - \cos 20° = 0.06$. As result a shift of $\mathrm{P}_\mu \xi$ value will be much less than 10^{-5}.

The cloud muons from 1AT1 target born from pions with a momentum $\mathrm{p}_\pi \approx 60$MeV/c decaying between the 1AT1 and the first bending magnet (total length is $\approx$ 2m). The muons flying out upstream and have an appropriate momentum $\mathrm{p}_\mu \approx 30$MeV/c. Time of flight of the pions between 1AT1 and the first bending magnet is $\approx$ 13ns. Total contamination of the cloud muons is 1% for a graphite target [8]. Cloud muon contamination for standard Be 1AT1 target has been measured [12]. That is about 9%(PSM) with muon polarization about $\mathrm{P}_\mu = +0.3$ in contrast with $\mathrm{P}_\mu = -1$ for surface muons. The cloud muons therefore sufficiently reduce the P_μ value of the surface muon beam. They are distributed inside a time interval $(0 - 13)$ns between proton beam pulses structure with 43ns periodicity. We are selected a time window $\approx$ 16ns long between the nearest pulses. Non-surface muon contamination was $6.7 \cdot 10^{-5}$(PSM)(Table 2) in this "usable" window. The total muon polarization equals to $1 - P_\mu = 8.3 \cdot 10^{-5}$ because the cloud muon polarization equals to $+0.3$.

Cloud muons from the slit S0 appear because high-energy pions with $\mathrm{p}_\pi \approx$100MeV/c from the target are slowed down to $\approx$60MeV/c by the S0 slit wall with thickness 8mm of Cu. Then, the slow pions can produce cloud muons in space of $\approx 0.5m$ length between S0 and the first bending magnet. Their time of flight is $\approx 3ns$. The above "usable" window has rejected these cloud muons from S0. We see additional methods for the cloud muon elimination. First, we are planning to change the 8mm Cu S0 walls on 0.5mm of Al ones. π^+-production cross-section by protons is 4 times less for p = 60MeV/c than for p = 100MeV/c [13]. That should decrease the cloud muon contamination in 4 times. Second, the cloud muons have a big emittance and the muon counter (TEC) on entrance of the E614 magnet will reject them.

We propose pessimistically that $(1 - \mathrm{P}_\mu) = (8.3 \pm 2) \cdot 10^{-5}$ because the non-surface muon contamination. The non-surface muons in the "usable" window have $\mathrm{P}_\mu \approx -1$ with high probability because we can see only one mechanism for their formation$-$a forward $\pi \to \mu$ decay of very slow pions in space between the target and the S0. The muons have $\mathrm{p}_\mu \approx 30$MeV/c and $\mathrm{P}_\mu \approx -1$, therefore they decreases the total polarization much less then cloud muons with P_μ =+0.3. The above estimation $(1 - \mathrm{P}_\mu) = (8.3 \pm 2) \cdot 10^{-5}$ will be revised after a direct measurement of the non-surface muon polarization inside the "usable" window.

3.1.3. Proton beam shift ($\pm$ 2mm) on the production target.
A vertical displacement of the proton beam on 1AT1 target of $\pm$ 2mm will result in a $\Delta\theta = \pm 2$mrad change in the muon beam direction at the final focus. This directly corresponds to a $(1 - \mathrm{P}_\mu)$ shift of $2 \cdot 10^{-6}$. It also leads to a $\pm$2mm transverse displacement of the muon beam in the fringe field area at the entrance to the solenoid and thus causes an additional increase of $(1 - \mathrm{P}_\mu) = 10^{-5}$. The present instrumentation in BL1A is sensitive to 0.5mm shifts in the position of the proton so that maintaining stability below 2mm is possible. For the existing 1AT1 target (see Fig.6) a 2mm proton beam shift in the horizontal plane not only adds to the fringe field depolarization as described above but may also change the mean value of the muon beam momentum. For a "rotated" target a horizontal shift will only affect the surface muon beam rate.

We will install the "rotated" target for the $\mathrm{P}_\mu \xi$ measurement to exclude the momentum

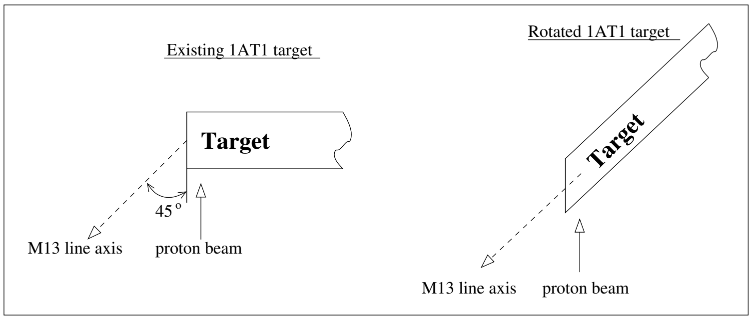

Figure 6: Sketch of the existing and rotated 1AT1 target.

change. A muon counter as described in section "Fringe field depolarization of muon" will measure each muon trajectory independently from a possible proton beam shift. A possible error of P_μ is included in the section.

3.1.4. Stability of the M13 settings to provide $\sigma(\Delta P_\mu) = 10^{-5}$ of the muon beam. M13 beam-line parameters influence on a central momentum p_0 of the surface muon beam. The momentum changing shifts the P_μ value. According to [11] $\Delta p/p_0 = \pm 0.03\%$ corresponds to $\sigma(\Delta P_\mu) = \pm 10^{-5}$. The influence of beam-line parameters on the p_0 value was measured in [7]. Three first columns in the Table 3 are copies of the Table II of [7]. The fourth column is added.

Table 3: Correlation of M13 beam-line parameters and transmitted momentum (see [7]) (Table II). "Least count" refers to the resolution of the digital beam-line control system when setting a given parameter.

Parameter	Least count	Δp/p, (%)	Instability value corresponds to $\sigma(\Delta P_\mu) = 10^{-5}$, ($\Delta p/p_0 = 0.03\%$)
1AT1 spot moved	≈1mm	<0.024	≈1mm
Horiz. jaw center	1mm	−0.002	15mm
SL1 center	0.1mm	−0.005	0.6mm
SL1, SL2 width	0.1, 0.1mm	0.0000	–
SL2 center	0.1mm	0.005	0.6mm
Q1 current	0.5%	0.002	7%
Q2 current	0.8%	0.012	2%
Q4 current	0.5%	0.002	7%
Q6 current	1%	0.013	2.3%
Q7 current	0.8%	0.017	1.4%
B2	0.05%	0.06	0.025%

M13 beam-line power supply stability was measured during 530 hours. Results are presented in Table 4.

One can see from Table 4 that the stability of B2 power supply only must be improved.

Table 4: Power supply instability during 530 hours.

Element	Q1	Q2	B1	Q3	Q4	Q5	B2	Q6	Q7
Long time instability (($\lvert$max. − min.$\rvert$/mean) $\cdot 10^{-4}$)	1.8	3.2	0.6	3.2	5.0	14.2	8.0	5.6	15.2

We will improve the quad and bending magnet power supply stability to level of 10^{-3} and 10^{-4} respectively to exclude their influence on P_μ value at level of 10^{-5}. Quad and bending magnets will be instrumented by Hall and NMR probes correspondingly.

3.2. Fringe field depolarization of muon.

Both the surface beam emittance and its distortion by a fringe field on entrance of E614 magnet define a possible decreasing of stopped muon polarization. M13 beam line simulation and optimization has been done using REVMOC and TRANSPORT code [14], GEANT [15] and ZGOUBI [16, 17] packages. A beam divergence θ defines an average muon polarization: $(1 - P_\mu) = 1 - \cos\theta$. A beam with emittance of 130π mm·mrad and θ=10mrad can be received at $1500s^{-1}$ and proton current of 100μA according to the above estimations and experimental results from M15 beam line running [18]. Muon polarization of such beam is $(1 - P_\mu) \approx 5 \cdot 10^{-5}$ that satisfy to E614 requirements.

Change of Z−component of muon spin by a fringe field on entrance of the magnet has been analyzed for a beam with different emittance and angle divergence θ [5, 19]. OPERA−2D and OPERA−3D packages have been used for the field calculations, and GEANT − for muon spin tracking, taking to account all interactions of muon with E614 detector. Calculations have been done for magnetic field B = 2T in the magnet center. Value of $(1 - P_\mu)$ in the stopping target varies from $4 \cdot 10^{-4}$ to $9 \cdot 10^{-4}$ for different kinds of the muon beam.

A muon counter has been proposed [6] to measure a trajectory of each incoming muon before the fringe field area where $B \approx 0$. The counter has space and angle resolution about 50μm and 4mrad respectively. Change of $(1-P_\mu)$ value by the fringe field can be calculated for each muon trajectory [5, 6] using the calculated or measured fringe field distribution. A map of the fringe field will be measured with accuracy of 1G and compared with the calculated one. According to [5] 24% of muons have $(1 - P_\mu) < 2 \cdot 10^{-4}$. Muons with a small depolarization will be selected in off-line regime using the muon counter data. We estimate a systematic error as $(1 - P_\mu) = (20 \pm 3) \cdot 10^{-5}$.

3.3 Muon depolarization due to muon stops in PC(−1).

About 7% of muons stop in PC(−1) gas. Muon polarization was measured in CF_4/ISO gas at B = 0 − 3T using HELIOS magnet and M15 beam line. $P_\mu = 0.985$ at B = 2T. It means the stopped in PC(−1) muons will decrease the total muon polarization to $(1-P_\mu) \approx$

$7\% \cdot 0.015 = 10^{-3}$. Amplitude cut of energy loss in PC(−1) and PC(−2) [2] decreases the muon stops to 0.6 % level. The total muon polarization is $(1 - \mathrm{P}_\mu) = (12 \pm 3) \cdot 10^{-5}$.

3.4 Muon deceleration and termalization.

Surface muon with original energy of 4.12MeV slowing down in matters goes through three consecutive stages: (i) scattering with (non-polarized) electrons; (ii) cyclic spin and charge exchange; (iii) thermalization regimes. We should try to estimate a possible muon depolarization in each stage beginning from last one.

3.4.1. Depolarization of thermal muon in metal at B = 2T.
In many nonmetals a thermalized μ^+ forms a neutral hydrogen-like atom called muonium − Mu ($\mu^+ e^-$), capturing a non-polarized electron of the matter. After that a dependence $\mathrm{P}_\mu(\mathrm{t})$ is described by frequencies of transition between different Mu states with different quantum numbers $\mid \mathrm{m}_\mu \mathrm{m}_\mathrm{e} >$, interactions with electrons and nucleus momentums of the matter, chemical Mu reactions, and value and direction of an external magnetic field. The $\mathrm{P}_\mu(\mathrm{t})$ behavior is a subject of μSR-method. Most important fact for E614 is a possibility of fast μ^+ spin depolarization during time of $\tau \approx 0.2$ns corresponding to the hyperfine frequency $\nu_0 = 4463$MHz between Mu states. The muon depolarization can be suppressed sufficiently by the longitudinal magnetic field B = 2T. But unfortunately, one can not calculate the real $\mathrm{P}_\mu(\mathrm{t})$ value at B = 2T because a microscopic theory of muon behavior in nonmetals does not exist. Muon in a nonmetal can form a paramagnetic complex with molecules during its slowing down (so-called "hot" chemical reactions). The paramagnetic complex can depolarize the muon spin very rapidly.

A thermalized muon in metals occupies a center of a corresponding crystal cell as that was confirmed in many μSR references. High-energy muon creates defects in a matter. The paramagnetic defects can produce sufficient magnetic fields on the stopped muon. Average distance between the stopped muon and the last atom displacement produced in graphite, for example, is $9000\mathring{A}$ according to reference [20]. We believe a contribution of the effect on P_μ value is negligible.

In metals the μ^+ is thermalized in a quasifree state because the conductive electron concentration $n \approx 10^{23}\mathrm{cm}^{-3}$ in normal metals effectively screens the μ^+ from interactions with individual electrons. Muon forms so called Kondo impurity (see, for example [21]) in a metal with characteristic temperature T_K. Conductive electrons completely screen the muon charge at $\mathrm{T} < \mathrm{T_K}$, and a muon spin depolarization stops because the muon interacts simultaneously with the non-polarized electron cloud.

Muonium like atom can form at $\mathrm{T} > \mathrm{T_K}$. The muon spin will be depolarized by a cyclic exchange between the electron of muonium with non-polarized conductive electrons. The exchange frequency ν can be easy calculated at $T \gg \mathrm{T_K}$. This picture corresponds to free muonium atom surrounded conductive electrons and $\nu = \sigma_\mathrm{e} \cdot \mathrm{v} \cdot \mathrm{n} \cdot \mathrm{kT/E_F}$, where $\sigma_e \approx 10^{-15} cm^2$ is cross-section of changing spin interaction between electron of the muonim and conductive electrons; $\mathrm{v} \approx 10^8 \mathrm{cm} \cdot \mathrm{s}^{-1}$ and $\mathrm{n} \approx 10^{23}\mathrm{cm}^{-3}$ are velocity and density of conductive electrons in a normal metal; $\mathrm{kT/E}_F$ is a portion of the electrons which can be scattered with spin flip; $E_F \approx 10$eV is Fermi energy of conductive electrons. Result is $\nu \approx 3 \cdot 10^{13}$s^{-1} at $T = 300K$. Muon spin depolarization time is $T_1 = \nu/\pi^2\nu_0^2 \approx 1.5 \cdot 10^{-7}$s $= 150$ns at T $= 300$K according to [22]. Value of T_K in normal metals is more than 300K therefore a very slow muon depolarization with $T_1 > 1$ms was found in all normal metals at T=300K in μSR experiments. Let us to remark that the T_1 estimation is very pessimistic because the value ν_0 in all investigated matters with conductive electrons is smaller then the vacuum value of 4463MHz according to μSR experiment results. For example the $\nu_0 = 230$MHz was measured in antimony [23]. As result, $T_1 > 6$ms was observed in the Sb at B=1kG.

The slow muon depolarization in a metal introduces P_μ error because we will see a time-dependent spin relaxation P_μ(t). To be measured value of P_μ corresponds to P_μ(t $= 0$). This value can be calculated from time analysis of Michel spectrum. The statistical error of P_μ was $\pm 8 \cdot 10^{-4}$ in reference [8]. At total statistics of 10^9 muon decay the error is $(1 - P_\mu) = \pm 4 \cdot 10^{-5}$.

Muon spin relaxation is caused by nuclear magnetic moments. The relaxation time T_2 measured by μSR method is more than 3μs for all investigated metals. The nuclear magnetic moments induce a magnetic field $\approx 2 - 4$G on muon. The longitudinal magnetic field B=2T decreases sufficiently the relaxation. Authors of reference [8] have suggested that the relaxation time T_1=4.6ms, observed in Al, can be explained by the decreased interaction. A possible statistics error of P_μ is inserted in the previous estimation $(1 - P_\mu) = \pm 4 \cdot 10^{-5}$.

Admixtures of ferromagnetic metals can produce magnetic field on a stopped muon. The atoms with an unpaired electron moment are in a paramagnetic state in a normal metal. It means the moment relaxes with a frequency $\approx 10^{13}$s^{-1}. The relaxation drastically decreases a possible influence on the muon spin. It is confirmed by a slow time ($> 10\mu$s) of muon depolarization in pure ferromagnetics at temperatures above Curie point in many μSR experiments. A possible slow muon relaxation in a sample with the ferromagnetic admixtures can be corrected as that was described above. Muon stopping targets from Al and C contain ≈ 1ppm of the ferromagnetic impurities. Be target contains ≈ 300ppm of Fe.

3.4.2 Muon depolarization during the cyclic charge and spin exchange regime.
Successive production and stripping of muonium atom Mu (μ^+e^-) begins after slowing down of surface muon to energy T < 3keV when a muon can form the Mu atom. This regime ends at T $\approx 20 - 200$eV when the Mu atom can not be stripped by interactions with a matter [24, 25, 26]. Value of a possible muon depolarization depends first of all on the deceleration muon time τ_D from 3keV to 20eV. Different authors give different values of τ_D. It is 10^{-13}s according to [24], $5 \cdot 10^{-13}$s $-$ [25], 10^{-12}s $-$ [26]. Calculation of the τ_D from muon range vs energy curve in Ni [27] gives $5 \cdot 10^{-14}$s. Calculation of the τ_D for Al by SRIM$-$2000.39 package [28] gives $\tau_D \approx 3 \cdot 10^{-13}$s from 10keV to 10eV. The package works correct till the kinetic energy T $= 10$eV for a primary particle and secondary ones. Authors of reference [29] have calculated muon range dependence in Al from the muon energy using slightly different code [30]. They have remarked that "The measured energy dependence agrees well with simulated values". Besides that we will use most pessimistic value of $\tau_D = 10^{-12}$s. M. Senba [31] (Fig.13b) have calculated muon depolarization in this regime for gases. According to the calculations the muon polarization is $(1 - P_\mu) = 3 \cdot 10^{-4}$, if the muon forms muonium with antiparallel spins of muon and electron, and keeps this state during the all $\tau_D = 10^{-12}$s.

Obviously, it is an overestimation because muons form also muonium with parallel muon and electron spins in a matter with non-polarized electrons. $(1 - \mathrm{P}_\mu)$ is zero for this case. Total value of $(1 - \mathrm{P}_\mu) \approx 1.5 \cdot 10^{-4}$. Obviously also, that several acts of the production and stripping of the muonium will decrease the $(1{-}\mathrm{P}_\mu)$ value. An interaction of muon with conductive electrons has not been considered in [31]. We have estimated in Table 5 the spin exchange interaction effects according to the above formula for thermalized muons.

Table 5: Muon depolarization during deceleration.

	Conductive electron density n, $(10^{23}\mathrm{cm}^{-3})$	Fermi energy $\mathrm{E_F}$, (eV)	Spin exchange frequency ν, $(10^{12}\mathrm{s}^{-1})$	$(1 - \mathrm{P}_\mu)$ (10^{-5})
Al	1.81	11.7	36.1	0.7
Be	2.47	14.3	42	0.6
Graphite	$\approx 3 \cdot 10^{-5}$	≈ 0.02	0.3	15

We proposed most pessimistic case: $\tau_D = 10^{-12}$s and $\nu_0 = 4463$MHz, for the calculations. The table demonstrates that the spin exchange of conductive electrons with miuonium atom decreases sufficiently the $(1{-}\mathrm{P}_\mu)$ values for Al and Be, and does not change practically the $(1 - \mathrm{P}_\mu)$ value for graphite. Acts of forming and stripping of muonium during $\tau_D = 10^{-12}$s will increase the ν value and decrease the $(1 - \mathrm{P}_\mu)$ value more. Therefore maximal $(1 - \mathrm{P}_\mu)$ values are presented in the table.

Comparison of experimental values of $(1 - \mathrm{P}_\mu\xi)$ for Al, Be, and graphite may be a direct method for confirmation of the deceleration muon contribution to total muon depolarization. Case $\mathrm{P}_\mu\xi(\mathrm{Al}) = \mathrm{P}_\mu\xi(\mathrm{Be}) = \mathrm{P}_\mu\xi(\mathrm{graphite})$ means that the above depolarization is very small because in graphite $\nu_0 \ll 4463$MHz or/and $\tau_D \ll 10^{-12}$s. Case $\mathrm{P}_\mu\xi(\mathrm{Al}) = \mathrm{P}_\mu\xi(\mathrm{Be}) > \mathrm{P}_\mu\xi(\mathrm{graphite})$ will confirm the above calculations. The depolarization difference of $1.4{\cdot}10^{-4}$ equals practically to statistics error 10^{-4} of $\mathrm{P}_\mu\xi$ for 10^9 events. Case $P_\mu\xi(Al) \neq P_\mu\xi(Be)$ means that we did an experimental mistake. We would like to propose preliminary a very conservative value of $(1 - \mathrm{P}_\mu) = (5 \pm 2) \cdot 10^{-5}$ for Al and Be during the muon deceleration time.

3.4.3. Muon scattering with non-polarized electrons.
Decreasing of surface muon polarization by scattering with non-polarized electrons during slowing down from 4.12MeV to 3keV has been calculated in reference [8]. It is $(1 - \mathrm{P}_\mu) = (1.5 \pm 0.2) \cdot 10^{-5}$.

3.5 Imperfections of the detector assembly.

3.5.1. Basic geometrical imperfections of the detector.
The influence of systematic deviations of the PDC assembly from the ideal was studied by using Monte Carlo vacuum helices (energy loss and multiple scattering turned off) for positrons with momentum 50MeV/c. Angles were uniformly distributed in the range θ=

$10-60°$. Wire plane spacing was changed from 4mm to 4mm$(1+\beta)$. Positron helixes in the PDC assembly were simulated (without energy losses). Helixes were reconstructed assuming β=0. The results indicated that an accumulated relative deviation $\beta = 5 \cdot 10^{-4}$ from a designed value along any axis X, Y or Z of the assembly introduces the following shifts of Michel parameters: $(\rho - 0.75) = \pm 5.2 \cdot 10^{-5}$, $(\mathrm{P}_\mu \xi - 1) = \pm 3 \cdot 10^{-5}$, $(\delta - 0.75) = \pm 5.4 \cdot 10^{-5}$. Such deviation value corresponds to an energy calibration shift of $\mid \Delta \mathrm{E}_0 \mid = 10$keV at the $\mathrm{E}_{max}= 52.831$MeV of the positron spectrum and reconstructed angle shift of $\mid \Delta\theta \mid = 5 \cdot 10^{-4}$. The deviation can appear because an average distance between wires in PDC planes is 4mm + 2μm systematically instead of 4mm, for example, or the distance between nearest PDC planes is 4mm + 2μm systematically instead of 4mm, or the deviation β=5$\cdot$10^{-4} is between X(Y) and Z axis units. Random errors of the β value in range $\beta = \pm 4 \cdot 10^{-3}$ contribute an error less than 10^{-5} to the Michel parameters, but the confidence level of a reconstructed helix is CL < 0.5 if $\mid \beta \mid > 5 \cdot 10^{-3}$ (it corresponds to 20μm of a wire random spread).

Preliminary description and test results of the PDC chambers presented in reference [32].

An accuracy of basic elements used for the assembly manufacturing defines the precision of the assembly. The basic elements are winding table, glass rulers for wire stretching defining the distance between wires, Cital spacers (4, 20 and 40mm thickness) defining a distance between planes, Cital spacers (1.997mm thickness) defining a distance between wire and cathode planes. Non-parallelism of the winding table surface is better than 0.5μm. All Cital spacer thickness were measured with accuracy of $\pm 0.3 \mu m$ [33]. Measured deviation between X(Y) and Z axis unit is $\beta < 1.25 \cdot 10^{-4}$ [34]. Distances between wires were measured for all manufactured PDC planes. An example of the distance distribution is presented on Fig.7. Average distance < s > between nearest wires is $| < s > -4mm \; | < 0.1 \mu$m with statistical spread of $\sigma_s = 2.4 \mu$m of individual wires. These above imperfections are about $\beta = 1.25 \cdot 10^{-4}$. It corresponds to following shifts the Michel parameter: $(\rho - 0.75) = \pm 1.4 \cdot 10^{-5}$, $(\mathrm{P}_\mu \xi - 1) = \pm 1 \cdot 10^{-5}$, $(\delta - 0.75) = \pm 1.4 \cdot 10^{-5}$.

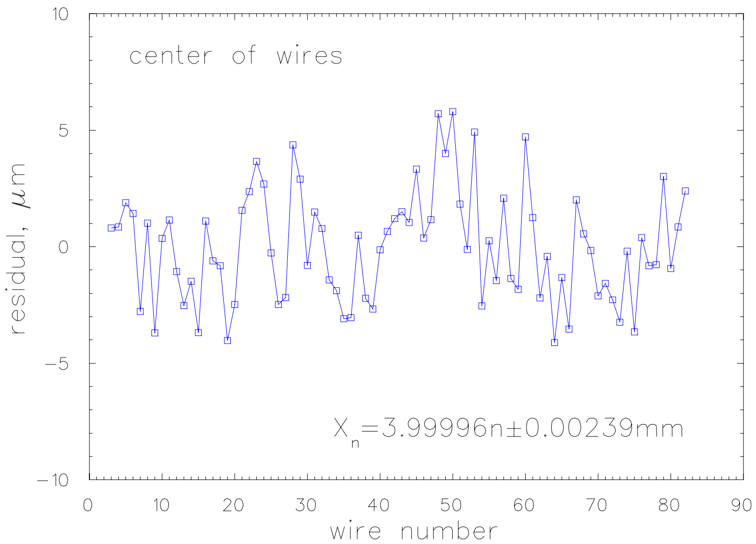

Figure 7: Residual distribution of distance between wires in DC plane #033DC.

The above imperfections of the detector we will name as the basic ones. The above estimations mean that we need to know a position of each wire in 3D-space with very high accuracy. Different kind of systematic errors appear even without the basic imperfections. There is an influence on Michel parameters of pressure, temperature, gap value between wires and cathode plane, Lorentz drift angle at B = 2T. We should demonstrate those much weaker accuracy requirements for these imperfections ("extra" imperfections) can be accepted for a correct measurement of Michel spectrum. We will begin from the Lorentz drift angle influence because most detailed Monte Carlo analysis for this case been done.

3.5.2. Lorentz drift angle in DME gas.
The Lorentz drift angle in DME gas is less than 9° at B = 2T [35]. The following simplified simulation model was used [10]. Distances of closest approach of a vacuum helix to hit wires d_i (DOCAs) were calculated first. Local Lorentz drift angle $\vartheta_{\rm i,L}$ at the points of closest approach were than computed to take into account the dependence of Lorentz drift angle component on the angle between the electric E and the magnetic B field $\vartheta_{\rm L} = \vartheta_{\rm L,max} \cdot \mid \sin({\rm E},{\rm B}) \mid$ assuming a constant (maximum) Lorentz angle $\vartheta_{\rm L} = 9°$ and simple radial direction of electrostatic field in the PDC cell. Finally, true DOCAs $\rm d_i$ were replaced on longer drift distances $d_{i,L}$=$d_i/\cos\vartheta_{\rm i,L}$ smeared with gaussian PDC resolution. The modified χ^2 was minimized to find parameters of the helix. Only the first 4 PDC pairs were used in the helix fit.

To avoid masking the Lorentz drift effect on track reconstruction the PDC resolution in the simulation was assumed to be $\sigma_{\rm PDC} = 0.5\mu$m instead of a realistic 50μm value. Results for the deviation of the mean reconstructed energy $<\Delta{\rm E}>=<{\rm E_{fit}} - {\rm E_0}>$ are presented on Fig.8 where the error bar on each point represents the uncertainty of the mean (for about 1500 events per point). As one can see from Fig.8, maximum deviations $|\Delta{\rm E}| \approx 100$keV are observed at small polar angles $\vartheta = 9.9°(\cos\vartheta = 0.985)$ when positrons are emitted from a point source ($\sigma_{\rm x} = \sigma_{\rm y} = 0$) at fixed polar angle ($\varphi_0 = 0$). The deviation of the mean energy drops drastically ($| < \Delta{\rm E} > | < 7$keV at $\cos\vartheta = 0.985$) due to averaging when one considers a real distributed positron source spot ($\sigma_{\rm x} = \sigma_{\rm y} = 1$cm, $\varphi_0 = 0$) from the stopping target. For a smaller Lorentz angle, $\vartheta_{\rm L,max} = 3°$ (or, equivalently, if one corrects drift distances in STR for Lorentz drift with 10% accuracy) the same averaging over source spot gives $|<\Delta{\rm E}>| < 0.6$keV. $|\Delta{\rm E}|$ becomes negligible at $\cos\vartheta < 0.9$. Similarly, deviation of the reconstructed polar angle is maximal for a point source and fixed azimuthal angle ($\Delta(\cos\vartheta) = |\cos\vartheta - \cos\vartheta_0| \approx 7 \cdot 10^{-5}$ at $\cos\vartheta_0 = 0.985$ and $\sigma_{\rm x} = \sigma_{\rm y} = 0, \varphi_0 = 0$) and drops to $\Delta(\cos\vartheta) < 2 \cdot 10^{-6}$ for a distributed source $\sigma_{\rm x} = \sigma_{\rm y} = 1$cm, $\varphi_0 = 0$. PDC resolution $\sigma_{\rm PDC} = 50\mu$m masks the effects, but the deviation values are remain.

Fig.9 presents the reconstructed energy spectrum from an original spectrum that was flat in range 20−50MeV. The total number of simulated events was 10^5. For an isotropic original spectrum this would correspond to a full statistics $\approx 10^{12}$ in 4π solid angle. As one can see from Fig.9, χ^2 values in the case $\sigma_{\rm x} = \sigma_{\rm y}$=0, $\varphi_0 = 0$ are significantly beyond their natural limits χ^2 =NDF $\pm\sqrt{2{\rm NDF}}$, i.e. systematic errors in the spectrum are higher than statistical errors. χ^2 values for a distributed source ($\sigma_{\rm x} = \sigma_{\rm y}$=1cm, φ_0=0) are within their natural limits, indicating that systematic errors from Lorentz drift effect are small at total statistics 10^{12} in 4π solid angle.

A lengthening of the DOCA because the Lorentz drift effect can be described as $\Delta{\rm d}(\mu{\rm m}) =$

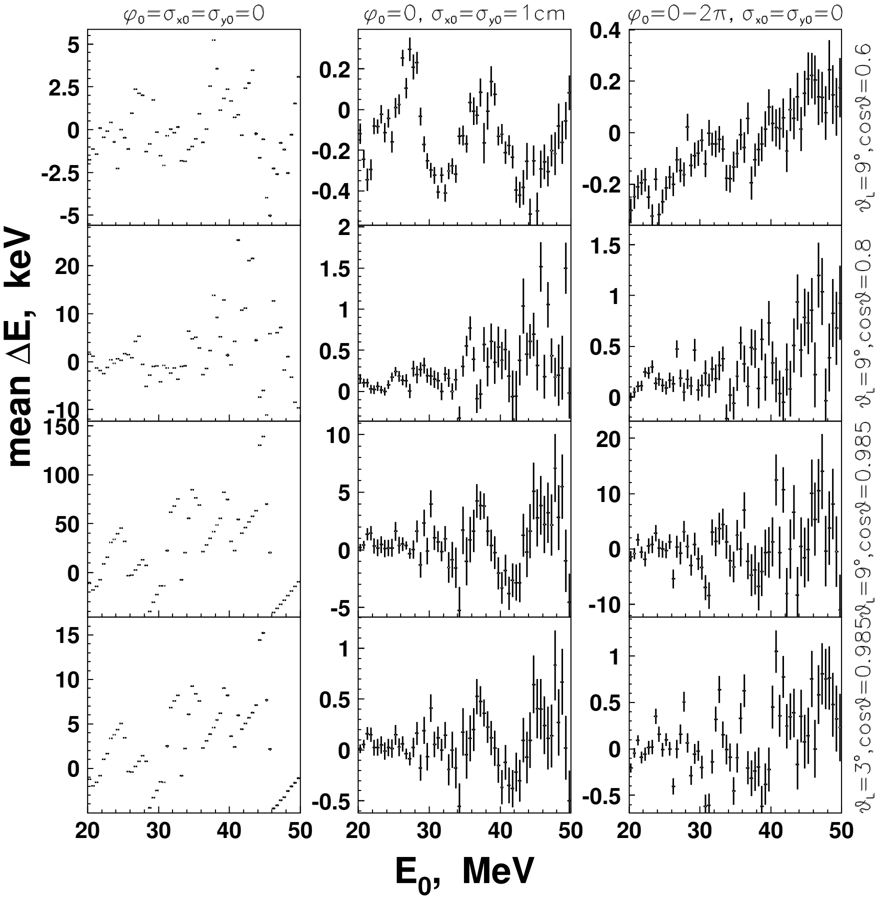

Figure 8: Mean shift of fitted energy $<\Delta\mathrm{E}>=<\mathrm{E}_{\mathrm{fit}}-\mathrm{E}_0>$.

$12\cdot\mathrm{d(mm)}/\cos\vartheta$ for DME gas at B = 2T ($\vartheta_{\mathrm{L,max}}=9^\circ$). Maximal deviation of d is $\Delta\mathrm{d}=24\mu\mathrm{m}$ at $\vartheta=0$ and d = 2mm. The above analysis demonstrates that even big deviation of 24μm does not change practically the reconstructed positron energy and angle, and therefore, does not shift the reconstructed Michel parameters. In contrast to this fact, the basic imperfections of the detector shift of Michel parameters on $\approx 5\cdot 10^{-5}$ level at $\Delta d=2\mu$m only. The insensitivity of Michel spectrum to the extra imperfection (Lorentz drift effect) is explained, as one can see from Figs.7, 8, by spreading of a positron source to real stopped muon spot with $\sigma_{\mathrm{x}}=\sigma_{\mathrm{y}}=1$cm. Obviously, the deviations are averaged because the spot size 1cm is larger the PDC periodicity of 4mm. Fortunately, average values of E_0 and ϑ_0 are remained with high accuracy.

Finally, we can not take into account Michel parameter shifts because the Lorentz drift angles in DME gas. Actually, the Lorentz drift angles were measured [35] for DME gas at B = 2T with accuracy of ±3%. The drift angles will be inserted in a reconstruction package because deviations more than 20μm worse a χ^2 value (see 3.5.1).

3.5.3. Gap between wire and cathode plane.
Influence of a wire-cathode distance deviation ΔD on shift Δd of a shortest distance between a wire and a positron helix was simulated by GARFIELD package. The calculated shift is

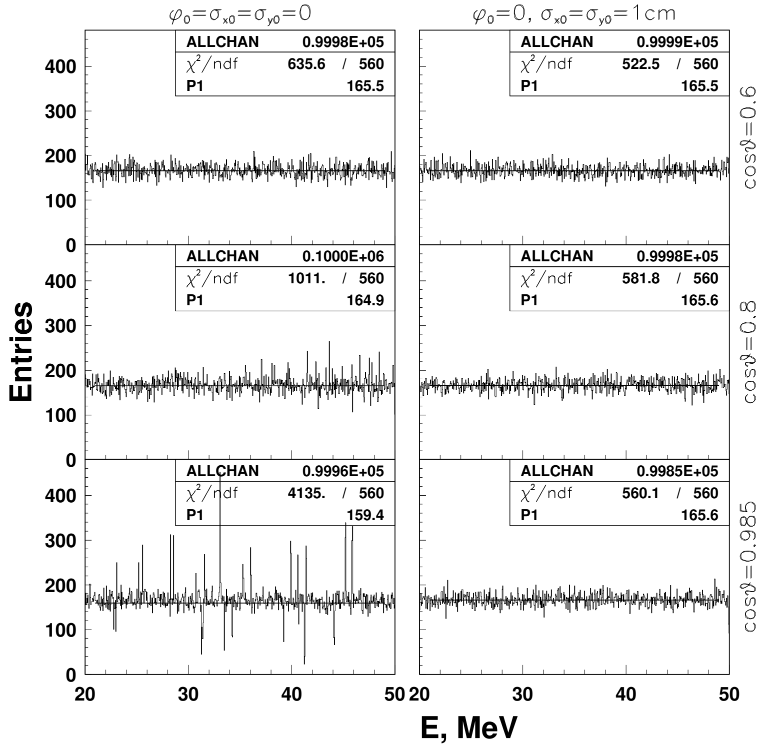

Figure 9: Reconstructed energy distribution and its fit to a constant (initial energy distribution was uniform). $\vartheta_{\mathrm{L,max}} = 9°$.

described roughly as $\Delta\mathrm{d}(\mu\mathrm{m}) = 0.06 \cdot \mathrm{d(mm)} \cdot \Delta\mathrm{D}(\mu\mathrm{m})/\cos\theta$, where θ is the projection of a positron helix polar angle on the plane orthogonal to the wire plane. This "extra" imperfection is described by the same dependence as the Lorentz drift effect. We have to provide $\mathrm{d_{max}} < 20\mu$m to conserve a correct χ^2 value at a helix reconstruction. The above $\Delta\mathrm{d_{max}}$ corresponds to $|\Delta\mathrm{D}| \approx 60\mu$m. Shift of Michel parameters will be $< 10^{-5}$. Now we are designing a tool for systematic measurements and adjustments of the D values in 24 points (through 15°) not far from the 24 screws of the G10 keeping the removable cathode plane to a permanent coil. Designed accuracy of the tool is $\pm 5\mu$m. We hope to adjust D values to $\pm 10\mu$m level.

3.5.4. Pressure difference between PDC gas and He gas.

Pressure difference between PDC gas (DME) and He gas around a PDC module will be supported with accuracy better than 6mTorr at a center of cathode plane. A mylar cathode foil with thickness 6μm between the gases will be deflected because a different density of DME and He gases. As result, the foil will have S−shape with maximal foil deflection $\Delta\mathrm{D} = +20\mu$m in the upper half of the foil and $\Delta\mathrm{D} = -20\mu$m in the bottom half. The deflection is zeroing along horizontal line goes through the cathode center if the pressure difference is zeroing also. But the horizontal line will move if the pressure difference is changing in range 6mTorr. Therefore the maximal deflection can reach $\Delta\mathrm{D} = \pm 40\mu$m according to estimations. The deflection appears only on outer foils of a PDC module. The deflection $\Delta\mathrm{D} = \pm 40\mu$m will change reconstructed distances between a helix track and wires on $\Delta\mathrm{d_{max}} \approx \pm 13\mu$m as it was analyzed before. The deflection value is less than 20μm which worse sufficiently the χ^2 value at a helix reconstruction. Finally, the pressure difference ("extra" imperfection also) does not shift the Michel parameters on level of 10^{-5}.

3.5.5. Temperature and pressure influence on PDC drift characteristics.
Temperature and/or pressure changing of DME gas in PDC planes shifts distance-drift time relationships according to GARFIELD calculations. Shift of the distance of closest approach can describe roughly as Δd(μm) = 1.5 $\cdot$ d(mm) per ΔT = 1°C. Temperature of the drift gas will be monitored with accuracy of 1°C and the distance-time relationship will be corrected. The inaccuracy 1°C corresponds to $\Delta d_{max} \approx 3\mu$m. This value does not worse the χ^2 value and does not shift the Michel parameters on level of 10^{-5} as previous "extra" imperfections. Pressure in Vancouver city changes on ±23Torr (maximum registered deviation) around 760Torr. Dependence of distance-time relationships can be described, according to GARFIELD calculations, as Δd(μm) = 0.6$\cdot$ d(mm) per 1Torr changing. It means the Δd_{max} value can reach ±28μm. Gas pressure will be monitored with accuracy of 6mTorr and the distance-time relationships will be corrected. The inaccuracy of 6mTorr causes a negligible shift of Michel parameters.

3.5.6. Wire sags.
We use (W-Re)Au wires with 15μm diameter and maximal length of 40cm stretched with a force of 30g. Maximal gravitational sag of a wire is about 1.3μm in center of wire length for a horizontally stretched wire. Wires in PDC planes of the E614 assembly arranged really in U and V directions with angle + and $-45°$ respectively relative to the vertical axis. Maximal value of the gravitational sag is about 1μm. The effect refers to a basic imperfection. An error in reconstruction helix can appear if a positron hits a wire in center of first PDC module, and then hits a wire in next module near wire edge where sag is zero. Minimal distance between the modules is 40mm. The above event gives angle shift $\Delta\theta \approx 1\mu$m/40mm $= 2.5\cdot10^{-5}$. This small angle deviation shifts the Michel parameters less than 10^{-5}.

3.5.7. Mutual orientation of PDC planes in the detector.
Design of the E614 assumes possible mutual shifts not more than 200μm between individual PDC chambers in (U, V) plane orthogonal to Z$-$axis. Assemble sizes along Z$-$axis defined by the basic elements using for the chamber production and assembling. The deviations in (U, V) plane can be defined by an illumination of the full detector with particles at B = 0. High energy pion beam with p = 150MeV/c from M13 channel illuminating a central area of the detector allows reconstruction of mutual shifts between U or V planes separately. Possible rotation angles between planes can be measured by an illumination of the detector far from Z=0. Unfortunately, so large shift (≈15cm) of the beam or the detector relative to each other is not possible. Therefore, a different method was proposed. A surface muon beam with big momentum spread $\Delta p/p \approx 5-7\%$ illuminates a central area of the detector. Muons stop in a stopping target and a remarkable part of them ($> 20\%$) stops in all chambers of the detector. Positrons decaying into 4π angle allow reconstruction of mutual imperfections of the detector inside its full volume. Monte Carlo program develops now for estimation of needed statistics to reconstruct the imperfections with accuracy 2μm. The same beam will be used for determination of relative distances between wires in a plane.

3.5.8. Geometrical acceptance.
The geometrical acceptance of the E614 detector has been studied in [36]. It was determined

that the acceptance is unity and uniform within the range $0.3 < x < 1$ and $0.3 <| \cos\theta |< 1$.

3.5.9. PDC inefficiency.
Both the PDC efficiency with DME gas and the PC efficiency with CF_4/ISO(80/20) gas have been measured in [3] at magnetic field B = 0 − 6T. The inefficiency $1-\epsilon$ of the both chambers was $< 10^{-3}$ (real numbers were $(1-\epsilon)_{\mathrm{DME}} \approx 1\cdot 10^{-4}$ and $(1-\epsilon)_{\mathrm{CF_4/ISO}} \approx 3\cdot 10^{-4}$). We should estimate the inefficiency influence on a helix reconstruction assuming the sliding technique with 5 pairs PDC 12345, 23456, 34567, 45678 (see Fig.1). A helix hits ≥10 wires per slide. The helix is described by 5 parameters. One more parameter−a common zero time t_0 for all hits, is needed for a fit because the time resolution of PC is about 2.5ns [3] that corresponds to a drift distance changing of $\approx 150\mu$m in DME gas as maximum. The t_0 value will be included in the helix fit also. An optimal value of t_0 will be fixed after the fitting and a helix will be fitted again for χ^2 minimization. An influence of the fixing will be checked by Monte Carlo to exclude possible helix parameter shifts at this procedure. Before that, we will believe pessimistically that t_0 value is the fitted parameter also. As result, we have ≥4 number degree of freedom (NDF) for the reconstruction. Probability to loss 2 hits is $< 10^{-5}$ at the inefficiency of $< 10^{-3}$. Probability to loss 3 hits is $< 10^{-7}$. These values are less that the statistic error of 10^{-5} for total statistics of 10^{10} events. We should suggest that we would be able to reconstruct a helix with ≥1 NDF. It means that the reconstruction is possible if even 3 hits are lost. This case appears very rarely at the inefficiency $< 10^{-3}$ for all wires in a slide with total number of 800 wires.

Different situation appears if "dead" wires or planes are among the 800 wires of a slide. Obviously, a one dead plane allows the helix reconstruction because a probability to loss 2 hits more is $< 10^{-5}$. Two dead planes allow the reconstruction in special cases only. We will request therefore not more than one dead plane among 16 planes for downstream or upstream part of the detector. Two dead wires in different planes allow the reconstruction as before. Three dead wires random placed in different planes do not possible the reconstruction of a helix going through the wires. Monte Carlo will estimate total statistics of such events. Before the estimations we should request not more than 2 dead wires per a slide (800 wires total).

The above analysis has been done for the sliding method. A developing now Kalman filtering [37] for a helix reconstruction uses all 16 planes. It corresponds to ≥32 NDF per track. Obviously, value of wire inefficiency can be $1-\epsilon \approx 10^{-2}$ or even less to reconstruct a helix. Also, more dead wire and plane number can be allowed for successful helix reconstruction by the Kalman filtering.

Inefficiency may result to the passage of the incoming μ through the upstream chambers. Going upstream decaying positron can hit wire cells crossed by the incoming muon before. The first problem arises from the possibility of mistaking a muon hit for that of a decay positron that is going upstream. In offline analysis the introduction of a 500ns wait time after the muon arrival before any positron hits are analyzed will lower the probability of making this mistake by a factor of ≈ 14 [38] (collect time is less than 500ns for 93% muons crossing a wire cell with DME gas). The second problem arises because of the long dead time ($> 20\mu$s) of a sense wire due to the slow dissipation of the ion cloud around the hit sense wire. The dead zone along the sense wire is about 0.5mm. We will try to estimate geometrically the possibility to reconstruct a going upstream positron helix without scattering of both the muon and positron suggesting that the muon goes along Z−axis at X = Y = 0 and stops at Z = X = Y = 0 in the stopping target (see Fig.1). A positron helix returns to Z−axis in one period. We will suppose pessimistically that the returned point coordinate Z (X = Y = 0) coincidences always with the muon dead zone in a chamber. The coincidence in a chamber is possible, as one can see from Fig.1, at fixed helix parameters E, θ, ϕ only. It means that 1 point with the dead time $> 10\mu$s is per 1 helix period. A positron helix also hits wires at $X = 0, Y \neq 0$ and $X \neq 0, Y = 0$ per 1 period far from X = Y = 0 point. The Y and X wires respectively have been crossed by the muon. It means that 2 more dead points are per 1 helix period with a probability of 93% that the points will be sensitive in 500ns wait time. Most difficult situation with a helix reconstruction because the dead points comes for a case with low positron energy and low polar angle simultaneously because more helix periods are putted up one slide 12345, 23456, 34567 or 45678, and number of hits is minimal ($\geq$10) per a slide. Let us to analyze the worst case a minimal positron energy (20MeV) and a minimal angle (10°) selected for Michel spectrum reconstruction. About 1.5 helix period is putted up one slide. It means that 1 permanent dead point and 3 temporally dead points are per a slide on the helix trajectory. Probability that all 3 temporally dead points remain dead ones in the 500ns is $(7\%)^3 \approx 3 \cdot 10^{-4}$. These events can not be reconstructed because 6 NDFs $(10 - 1 - 3 = 6)$ are for 6 fitted helix parameters. Let us remark that the problem exists only for the upstream part of the detector because the overlap between muon and positron tracks. The problem can be resolved obviously using more than 5 PDC pairs for the helix reconstruction. Kalman filtering method with 16 PDC planes should be used for the problem resolving. The method has a disadvantage − it requests $2^{16} \approx 64000$ independent fittings for $\approx 20\%$ of reconstructed events to resolve a left−right ambiguity compare with about 5000 independent fittings for the sliding method. Percentage of the events with E < 30MeV and $\theta < 20^\circ$ in the upstream Michel spectrum is about 1%. All upstream positron helixes did not reconstructed by the sliding method will be reconstructed using the Kalman filter technique. Percentage of such events will be much less than 1%.

A special case appears for an upstream helix with period of 4mm. The helix crosses Z−axis in all PDC chambers for the selected detector geometry with He gap of 40 or 60mm between the PDC pairs. It means that all positron hits coincidence geometrically with the incoming muon hits which kill all positron hits because the permanent dead zone is from the muon. Angle θ of such helix is minimal ($\approx 85^\circ$) at minimal positron energy E = 20MeV inside selected energy range 20MeV < E < 53MeV. Positron hits $\geq$10 nearest wires per plane therefore $\geq$100 original hits are per slide. This helix can be reconstructed of course in spite of the 10 hits killed by the muon track. θ is more than 85° at E > 20MeV. Let us remark that the all special cases with helix period of 4mm lie outside the selected range of 20MeV < E < 53MeV and $10^\circ < \theta < 60^\circ$. The special helix events with period of 4mm together with events having $< 10^\circ$ will analyze PDCs dense stack (Fig.1) to remove the events from collecting Michel spectrum.

In conclusion, possible detector non-homogeneity does not contribute Michel parameter errors more than 10^{-5}.

3.5.10. Creation of thin films on the surface of the stopping target.

Muon depolarization is possible in solid films, which can be formed on the surface of the stopping target. In [1] the thickness of such a solid film on the surface of PC anode wires was measured after an accumulated charge $\approx$ 5C/cm which corresponds to more than 10^{12} detected particles per 1cm of sense wire. The mixture CF_4/ISO (80/20) was used as a drift gas. The thickness of the film was $20\AA$. Surface muons provide a maximal total accumulated charge in a central area of the E614 ($X \approx Y \approx 0$) of PC(-2) and PC(-1) where muon losses exceed in $\approx$ 100 times positron energy losses. The accumulated charge per 10^{11} registered muons is $\approx$ 0.1C/cm. It corresponds to $0.4\AA$ of the film thickness, which is very small, and thus a negligible influence on muon polarization. The drift gas could permeate into pores and structure disturbances of a target foil. We will use Be and graphite target covered by a thin diamond like film without pores practically. Surface of high purity Al has not pores also.

3.5.11. PDCs misalignment ($<$ 0.1mrad) with respect to B direction.
A misalignment $\theta_{\rm PDC,B}$ between PDC assembly and the magnet axis will distort the Michel spectrum. The Michel spectrum is independent of azimuthal angle φ, but such a misalignment $\theta_{\rm PDC,B} \neq 0$ will introduce a φ dependence into the measured spectrum. With total statistics of 10^8 muon decays this artificial φ asymmetry can be measured to an angular accuracy of 0.1mrad and corrective adjustments will than be made. Shifts of Michel parameters because of a 0.1mrad misalignment are less than 10^{-5}. The above method can be used for the alignment. A different and more convenient method was proposed and tested also. A misalignment $\theta_{\rm PDC,B}$ means that a positron helix axis does not coincide with the perpendicular to PDC planes (Z$-$axis). A helix trajectory describes taking to account the misalignment angle. Fitting of the helix with the free parameter $\theta_{\rm PDC,B}$ allows experimental measurement of the misalignment value. Total statistics of greater than 10^4 events ($\approx$ 10s of running time) provide accuracy of $\sigma(\theta_{\rm PDC,B}) \approx$ 0.1mrad because angle resolution of the spectrometer at positron helix reconstruction is about 10mrad [10]. This second method allows practically online control of the $\theta_{\rm PDC,B}$ value during a beam running.

E614 detector is supported by the solenoid. Alignment the detector is provided in a wide range. Laser alignment system is designed and tested for the purpose [40, 41]. Accuracy of the system is $\pm 10\mu$m on length of $\approx$ 1m therefore the alignment will be controlled with accuracy of $\pm 10^{-5}$ in online regime.

3.5.12. Misalignment ($<$ 1mrad) of B with respect to the beam direction.
The possible misalignment of 1mrad will shift only P_μ value on $(1-\cos(1\mathrm{mrad})) < 10^{-5}$. An alignment will be accomplished by measuring the transverse component of muon polarization $P_\mu = \sin\theta_{beam,B}$ using ordinary μSR techniques at B=2T (muon precession period 3.5ns) before the PDC assembly is inserted into the solenoid. To measure the misalignment and make the required corrections and check the result could require substantial beam tune time, a reasonable estimate for a couple of iterations is 8 days on M13 at p = 29.6MeV/c at 100μA.

3.5.13. Deviation (10^{-4}) of magnetic field magnitude.
Magnetic field distribution in E614 magnet with the real iron yoke was calculated [19] using OPERA-3D package. The field deviation reaches 10^{-3} on outside ends of the detector. Magnetic field map will be measured also with accuracy of $\pm$1G. It corresponds to a relative error of $\pm 5 \cdot 10^{-5}$ at B = 2T. The map will be introduced at positron helix reconstruction.

We should believe conservatively $\pm 10^{-4}$ accuracy of the map. It corresponds to an energy shift ΔE = $\pm$5keV at E = 50MeV. According "Positron energy calibration" section that corresponds to follow parameter errors: $(0.75-\rho) = \pm 2.6 \cdot 10^{-5}, (1-\mathrm{P}_\mu) = \pm 1.5 \cdot 10^{-5}, (0.75-\delta) = \pm 2.7 \cdot 10^{-5}$. The value of B = 2T will be controlled with accuracy better than 10^{-4} during the experiment.

3.6. Positron energy calibration

The calibration of the detector at $x \to 1$ will be contained within the measured Michel spectrum. It was demonstrated in section "Peculiarities of the E614 detector" using the slide fitting technique that the energy calibration of the Michel spectrum can be fit to provide an energy calibration with an accuracy of $\pm$ 2keV [10]. The method has a big advantage because it provides the energy calibration for a real distribution of all stopped muons with total statistics of 10^9 events along Z−axis in the stopping target. It means that the obtained calibration can be directly used for the full Michel spectrum reconstruction. Any different calibration method, for example, using of $\pi \to e$ decay in stopping target, requests some corrections taking to account a difference between muon and pion stop distributions along Z−axis for these two separate experiments.

The energy calibration is not restricted to this $x \to 1$ point but can be assumed to apply over the full energy range $0.4 < x < 1$ since the E614 detector is a linear detection system because of the homogeneous magnetic field. Peculiarities of the Michel spectrum $d^2N/dxdcos\theta = N_1(x, \rho, \eta) \pm N_2(x, \delta) P_\mu \xi \cos\theta$ allow using of additional energy points for the checking of the calibration accuracy. The upstream and downstream part of the detector registers $N_{up} = N_1 + N_2 \cdot P_\mu \cos\theta$ and $N_{down} = N_1 - N_2 \cdot P_\mu \cos\theta$ respectively for a surface muon beam with $P_\mu = -1$. Analysis of $N_- = N_{up} - N_{down} = 2N_2(x, \delta) P_\mu \xi \cos\theta$ allows the calibration accuracy checking because the ratio $M = \partial/\partial x[N_-(x = 0.5)]/N_-(x = 0.75) = 16/9$ is independent of the Michel parameters $\rho, \eta, \mathrm{P}_\mu\xi$, and δ. An energy calibration error $\Delta \neq 0$ results in $\mathrm{M} = (16/9) \cdot (1 - \Delta/\mathrm{E}_{\max})$.

A Monte Carlo checked the energy calibration method. $2 \cdot 10^5$ positrons were generated by EGS4 and reconstructed for initial energies and angles in ranges $1 < x < 0.9$ and $0.4 < \cos\theta < 0.995$. The average energy corresponding to $x = 1$ was $< \mathrm{E}_{\max} >= (52.77 \pm 0.03)$MeV, very close to the correct value 52.831MeV. The conclusion is that the planar geometry of the E614 makes it possible to calibrate the energy scale with high precision. A higher statistics ($2 \cdot 10^7$ events) study would be expected to provide an energy calibration with an accuracy better than 4keV. Taking a conservative approach we have assumed that the energy calibration uncertainty will be 10keV. It corresponds to follow parameter errors: $(0.75 - \rho) = \pm 5.2 \cdot 10^{-5}, (1 - \mathrm{P}_\mu\xi) = \pm 3 \cdot 10^{-5}, (0.75 - \delta) = \pm 5.4 \cdot 10^{-5}$.

3.7. Response function.

The E614 detector may be logically separated into two parts. The first part, where the positron helix is not measured, consists of the stopping target, the PC($\pm$1) and PC($\pm$2), a helium gap and the cathode plane of the first PDC. Positron loses energy in collision and radiative interactions with this part. It can annihilate or be scattered back also. The all interactions distort the Michel spectrum on entrance of the coordinate part (PDC (± 1)) of the detector. The coordinate part does not distort a spectrum, as that has been demonstrated above in the section "Imperfections of the detector assembly". Maximum positron energy loss in the first part reaches 80keV for Al and 45keV for Be target at E=54MeV and $\theta = 60°$ (50keV and 35keV respectively at E=20MeV and $\theta = 60°$).

Influence of the positron annihilation and backscattering on the Michel parameters has been simulated by EGS4 package. The probabilities of annihilation $\varepsilon_{2\gamma}(x,\theta)$ and backscattering $\varepsilon_B(x,\theta)$ in the first part of the detector were computed. The exact formula of muon decay $\mathrm{d}^2\mathrm{N}/\mathrm{dxd}\cos\theta$ was multiplied by $\varepsilon_{2\gamma}(x,\theta)\cdot\varepsilon_B(x,\theta)$. The resulting distribution was randomized with total statistics 10^{11} events of muon decay in 4π solid angle. The randomized spectrum was fitted by $\mathrm{d}^2\mathrm{N}/\mathrm{dx}(\mathrm{d}\cos\theta)$. When $0.4 < x < 1, 10° < \theta < 60°, 120° < \theta < 170°$ the positron annihilation and backscattering results in the following corrections to parameters: $(0.75 - \rho) = 5 \cdot 10^{-5}, (1 - \mathrm{P}_\mu\xi) < 10^{-5}, (0.75 - \delta) = 10^{-5}$.

Michel spectrum after the first part of the detector was simulated by the EGS4 with 10^8 events. The resulting spectrum was fitted. We got the following parameter values: $(0.75-\rho) = \pm 1.2\cdot 10^{-3}, (1-\mathrm{P}_\mu\xi) = \pm 1.4\cdot 10^{-3}, (0.75-\delta) = \pm 5\cdot 10^{-4}$. Thus, the scattering processes shift the Michel parameters considerably. We will simulate by Monte Carlo the Michel spectrum with total statistics 10^9 events on entrance of the coordinate part of the detector. The spectrum distortion (response function) can be calculated with an accuracy of a simulating package. For example, the existing GEANT3 package has an inaccuracy $\pm 6\%$ at positron simulation in range of 10−50MeV. Taking to account the inaccuracy, we can reconstruct the Michel parameter values with precision: $(0.75-\rho) = \pm 7.2\cdot 10^{-5}, (1-\mathrm{P}_\mu\xi) = \pm 8.4\cdot 10^{-5}, (0.75-\delta) = \pm 3\cdot 10^{-5}$. The above inaccuracies can be decreased taking to account that cross sections of positron interactions in the range 20−50MeV are known with accuracy of $\pm 1.5\%$ according to references [42, 43]. We will believe pessimistically the accuracy of $\pm 3\%$. It corresponds to following errors of the Michel parameters: $(0.75 - \rho) = \pm 3.6 \cdot 10^{-5}$, $(1 - \mathrm{P}_\mu\xi) = \pm 4.2 \cdot 10^{-5}$, $(0.75 - \delta) = \pm 1.5 \cdot 10^{-5}$.

3.8. Online control of the E614.

We numerate below control settings of the E614 to fix the systematic errors.

• Proton beam position on 1AT1 target.
The present instrumentation in BL1A is sensitive to 0.5mm shifts in the position of the proton beam.

• M13 line elements.
Power supply of the quad and bending magnets will provide 10^{-3} and 10^{-4} current stability correspondingly. Hall and NMR probes to measure the beam element fields with accuracy of 10^{-3} and 10^{-4} respectively will be installed in quad and bending magnets.

• Muon beam emittance and direction.
Muon counter will measure the muon beam emittance and the beam direction relative to the E614 detector.

• Alignments.
Alignment of the detector−solenoid and solenoid−iron yoke systems will be controlled by laser tools with accuracy of 0.1mrad. Additional alignment checking of the detector−solenoid system will provide the positron helix axis reconstruction.
• Temperature and pressure.
Temperature and pressure of the drift gases will be controlled with accuracy of $0.3°C$ and 6mTorr respectively.

• The correction and error estimations are presented in Table 6.

Table 6: Correction and Error Estimations. Corrections and Errors with $> 10^{-5}$are presented.

	Discussed in section	Source of Correction or/and Error	$(1-\mathrm{P}_\mu\xi)$ (10^{-5})	$(0.75-\rho)$ (10^{-5})	$(0.75-\delta)$ (10^{-5})
1	3.1.1	Coulomb scattering of muons inside the production target	9 ± 2		
2	3.1.2	Non-surface muon contamination	8.3 ± 2		
3	3.2	Fringe field muon depolarization	20 ± 3		
4	3.3	Muon depolarization due to muon stops in PC(−1)	12 ± 3		
5	3.4.3	Muon scattering by unpolarized electrons	1.5 ± 0.2		
6	3.4.1	Slow depolarization of thermal muon in metal at B=2T	±4		
7	3.4.2	Muon depolarization due to muonium formation and stripping at $\mathrm{E}_\mu < 3$keV	5±2		
8	3.5	Imperfections of the detector assembly	±1	±1.4	±1.4
9	3.6	Positron energy calibration	±3	±5.2	±5.4
10	3.7	Response function	±4.2	±3.6	±1.5
11	3.5.13	Deviation(10^{-4}) of magnetic field magnitude	±1.5	±2.6	±2.7
12		Statistical errors for 10^9 events	±10	±5	±8

• Michel parameter errors:
$\sigma(\mathrm{P}_\mu\xi) = [\pm 10(\mathrm{stat}) \pm 8.5(\mathrm{syst})] \cdot 10^{-5}$.
$\sigma(\rho) = [\pm 5(\mathrm{stat}) \pm 7.0(\mathrm{syst})] \cdot 10^{-5}$.
$\sigma(\delta) = [\pm 8(\mathrm{stat}) \pm 6.4(\mathrm{syst})] \cdot 10^{-5}$.

References

[1] V.I. Selivanov, M.A. Vasiliev "Monte Carlo Simulation of Muon Stop Distributions in E614 Targets", TN−47, 14 September 2000.

[2] D.H. Wright "An Analysis of Energy Loss in the Prop. Chambers near Target", TN−22, 31 August 1998.

[3] Y.Y. Lachin, L.V. Miassoedov, I.V. Morozov, V.I. Selivanov, I.V. Sinitzin, V.D. Torokhov "Wire chamber as a fast, high efficiency and low mass trigger in high magnetic fields", Nucl. Instr. Meth. A361(1995)77−84; TN−20, 4 August 1998

[4] M.A. Quraan, J.A. Macdonald, J.M. Poutissou "Muon Trigger Scintillator", TN−26, 20 January 1999.

[5] B. Ramadanovic, D.H. Wright "Optimization of Muon Polarization in the M13 Beamline and E614 Detector", TN−31, 17 May 1999.

[6] Yu.I. Davydov, V.I. Selivanov "Design end Estimations of Muon Counter Parameters", TN−17, 25 May 1998.

[7] B. Balke, G. Gidal, A. Jodidio, K.A. Shinsky, N.M. Steiner, D.P. Stoker, M. Strovink, R.D. Tripp, J. Carr, B. Gobbi, C.J. Oram "Precise measurement of the asymmetry parameter δ in muon decay", Phys. Rev. D37(1988)587−617.

[8] A. Jodidio, B. Balke, J. Carr, G. Gidal, K.A. Shinsky, N.M. Steiner, D.P. Stoker, M. Strovink, R.D. Tripp, B. Gobbi, C.J. Oram "Search for right-handed currents in muon decay", Phys. Rev. D34(1986)1967−1990; ibid. D37(1998)237-238.

[9] S.E. Derenzo "Measurement of the Low-Energy End of the μ^+ Decay Spectrum", Phys. Rev. 181(1968)1854−1866.

[10] A.A. Khrutchinsky, Yu.Yu. Lachin, V.I. Selivanov "A Monte Carlo study of a precision magnetic spectrometer with planar geometry", Nucl. Instr. Meth. A396(1997)135−146; TN−19, 27 July 1998.

[11] R. Abegg, M. Comyn, M. Cooper, C. Gagliardi, D. Gill, P. Gumplinger, M. Hasinoff, R. Helmer, A. Khruchinsky, D. Koetke, Y. Lachin, J. Macdonald, R. Manweiler, L. Miassoedov, D. Mischke, J-M. Poutissou, R. Poutissou, N. Rodning, V. Selivanov, B. Shin, I. Sinitzin. S. Stanislaus, R. Tacik, V. Torokhov, R. Tribble, G. Wait, D. Wright "Precision Measurement of the Michel Parameters of μ^+ decay", E614 Proposal, July 1996, http://stoney.phys.ualberta.ca/ rodning/E614/.

[12] R. MacDonald "Summary of M13 Momentum Scans of Surface Muon Edge", TN−52, 8 March, 2001.

[13] R. Frosch, J. Loffer, C. Wigger "Decay of pions trapped in graphite", PSI preprint TM-11-92-01, 1992.

[14] N. Rodning "Revmoc and Transport Tunes", TN−32, 2 June 1999.

[15] B. Bock "Setting Up and Investigating the M13 Beam−line in GEANT for TRIUMF Experiment E614", TN−36, 30 August 1999.

[16] J. Doornbos "The tuning of M13 for TWIST, theory and some results", TN−51, December 20, 2000.

[17] J. Doornbos "Optimization of the M13 Surface Muon Beam for Experiment TWIST, and its Injection onto the Solenoid", TRIUMF, August 3, 2000, http://www.triumf.ca/people/doornbos/homepage.html/.

[18] V.I. Selivanov "Previous Experience of Beam Line Studies", TN−44, 25 May 2000.

[19] D.H. Wright "3−D Magnetic Field Calculations of the E614 Magnet", TN−40, 18 January 2000.

[20] D.K. Brice "Lattice atom displacements produced near the end of implanted μ^+ tracks", Phys. Lett., 66A (1978) 53−56.

[21] A.C. Hewson "The Kondo Problem to Heavy Fermions", Cambridge University Press, Cambridge 1993.

[22] A. Schenk, Muon Spin Rotation Spectroscopy, Adam Hilger Ltd., Bristol and Boston, 1985, p.128.

[23] T.M.S. Johnston, K.H. Chow, S. Dunsiger, T. Duty, R.F. Kiefl, E. Koster, W.A. MacFarlane, G.D. Morris, J. Sonier, D.L.I. Williams "The giant Knight shift on antimony: Evidence for a Kondo impurity", Hyperfine Interactions 106 (1997) 71−76.

[24] K.M. Crowe, J.F. Hague, J.E. Rothberg, A. Schenck, D.L. Williams, K.K. Yong "Precision measurement of the Magnetic Moment of the Muon", Phys. Rev., D5(1972)2145−2161.

[25] A. Schenk "Positive muons and muonium in matter", First Course of the International School of Physics of Exotic Atoms, Erice, 24−30 April 1977.

[26] J.N. Brewer, K.M. Crowe "Advances in muon spin rotation", Annual Reviews of Nuclear and Particle Science, 1978, v.28, p.239.

[27] E. Morenzoni "Low energy muons at PSI", Workshop on Applications of Low Energy Muon to Solid State Phenomena, February 17−19, 1999, Paul Scherrer Institute, Switzerland.

[28] J. Ziegler, SRIM2000−release 2000.39, http://www.research.ibm.com/.

[29] H. Glucker, E. Morenzoni, T. Prokscha, M. Birke, E.M. Forgan, A. Hofer, T.J. Jackson, J. Litterst, H. Luetkens, Ch. Niedemayer, M. Pleines, T.M. Riseman, G. Schatz "Range studies of low-energy muons in a thin Al film", Physica B 289-290 (2000) 658−661.

[30] W. Eckstein, Computer Simulations of Ion-Solid Interactions, Springer, Berlin, 1991.

[31] M. Senba "Muon spin depolarization in noble gases during slowing down in a longitudinal magnetic field", J. Phys. B31 (1998) 5233−5260.

[32] Yu. Davydov, W. Andersson, M. Comyn, P. Depommier, J Doornbos, W. Faszer, C.A. Gagliardi, D.R. Gill, P. Green, P. Gumplinger, J.C. Hardy, M. Hasinoff, R. Helmer, R. Henderson, A. Khruchinsky, P. Kitching, D.D. Koetke, E. Korkmaz, Yu. Lachin, D. Maas, J.A. Macdonald, R. MacDonald, R. Manweiler, G. Marshall, E.L. Mathie, L. Miassoedov, J.R. Musser, P. Nord, A. Olin, R. Openshaw, D. Ottewell, T. Porcelli, J-M. Poutissou, R. Poutissou, G. Price, M.A. Quraan, N.L. Rodning, J. Schaapman, V. Selivanov, G. Sheffer, B. Shin, F. Sobratee, J. Soukup, T.D.S. Stanislaus, G. Stinson, R.Tacik, V. Torokhov, R.E. Tribble, M.A. Vasiliev, H.C. Walter, D. Wright "Drift chambers for a precision measurement of the Michel parameters in muon decay", Nucl. Instr. Meth. A461 (2001) 68−70.

Maher Quraan "Test Chamber Calibration Code", TN−46, November 30, 1998.

[33] V.I. Selivanov "Results of Ceramic Glass Spacer Thickness Measurement", TN−18, 23 July 1998.

[34] V.I. Selivanov "Measurement of Cital Spacer Thickness by Glass Ruler", TN−45, 7 July 2000.

[35] B. Zhou, A. Marin, T. Coan, J. Beatty, S. Allen "Using Dimethyether as a Drift Gas in a high Precision Drift Tube Detector", Nucl. Instr. Meth., A287 (1990) 439−446.

[36] D. Wright "Monte Carlo Study of E614 Spectrometer Resolution and Acceptance", TN−2, 14 March 1997.

[37] M. Quraan "Maher's Talk on Kalman filtering", 4−6 May 2000 Collaboration Meeting.

[38] Yu.Yu. Lachin "GARFIELD study of two PDC cell types", TN−3, March 1997.

[39] R. Openshaw et. al. Nuclear Science and Nuclear Power Systems Symposium, Orlando, Nov. 9−11 1988.

[40] P. Kitching "Conceptual Design of Laser Alignment System", TN−27, 26 February 1999.

[41] G. Price "Laser Alignment System Studies", TN−38, 4 October 1999.

[42] S.M. Seltzer, M.J. Berger "Bremsstrahlung Spectra from Electron Interactions with screened atomic Nuclei and orbital Electrons", Nucl. Instr. Meth. B12 (1985) 95−134.

[43] L. Kim, R.H. Pratt, S.M. Seltzer, M.J. Berger "Ratio of positron to electron bremsstrahlung energy loss: An approximate scaling law" Phys. Rev. A33 (1986) 3002−3009.